

# Magnus-Induced Dynamics of Driven Skyrmions on a Quasi-One-Dimensional Periodic Substrate

C. Reichhardt and C. J. Olson Reichhardt  
*Theoretical Division, Los Alamos National Laboratory,  
Los Alamos, New Mexico 87545 USA*

(Dated: November 18, 2021)

We numerically examine driven skyrmions interacting with a periodic quasi-one dimensional substrate where the driving force is applied either parallel or perpendicular to the substrate periodicity direction. For perpendicular driving, the particles in a purely overdamped system simply slide along the substrate minima; however, for skyrmions where the Magnus force is relevant, we find that a rich variety of dynamics can arise. In the single skyrmion limit, the skyrmion motion is locked along the driving or longitudinal direction for low drives, while at higher drives a transition occurs to a state in which the skyrmion moves both transverse and longitudinal to the driving direction. Within the longitudinally locked phase we find a pronounced speed up effect that occurs when the Magnus force aligns with the external driving force, while at the transition to transverse and longitudinal motion, the skyrmion velocity drops, producing negative differential conductivity. For collectively interacting skyrmion assemblies, the speed up effect is still present and we observe a number of distinct dynamical phases, including a sliding smectic phase, a disordered or moving liquid phase, a moving hexatic phase, and a moving crystal phase. The transitions between the dynamic phases produce distinct features in the structure of the skyrmion lattice and in the velocity-force curves. We map these different phases as a function of the ratio of the Magnus term to the dissipative term, the substrate strength, the commensurability ratio, and the magnitude of the driving force.

PACS numbers: 75.70.Kw,75.25.-j,75.47.Np

## I. INTRODUCTION

There are numerous examples of systems that can be described as individual particles or a collection of particles interacting with a periodic quasi-one dimensional (q1D) substrate, including colloids on optically created q1D substrates<sup>1-4</sup> or q1D line pinning<sup>5-7</sup>, vortices in type-II superconductors with one-dimensional (1D) periodic thickness modulations<sup>8-14</sup>, and various frictional systems<sup>15</sup>. In the colloidal systems a variety of commensurate-incommensurate states can occur such as crystal, smectic, and disordered structures<sup>1-5</sup>. In vortex systems, under an applied driving force a series of peaks or dips in the critical depinning force can appear which are also associated with commensuration effects<sup>8-10,12</sup>. These systems, as well as other systems of particles interacting with two-dimensional (2D) periodic substrates, can exhibit a variety of depinning phenomena and dynamic phases, and can undergo transitions between different types of dynamic phases that produce changes in the configuration of particles and flow behavior as well as features in the velocity-force curves<sup>7,8,14-23</sup>. In a 2D overdamped system with a q1D periodic substrate, pinning-depinning phenomena and distinct dynamical phases appear only when the driving force is applied parallel to the substrate periodicity direction. If the drive is applied perpendicular to the substrate periodicity direction, there is no pinning effect from the substrate and the particles simply slide along the driving direction, resulting in a linear velocity-force curve.

In overdamped systems in the absence of a substrate,

individual particles move in the same direction as the applied driving force. In some systems, additional transverse forces can arise when a Magnus force term  $\mathbf{F}_M$  with the form  $\hat{z} \times \mathbf{v}$  is present, which causes a rotation of the particle velocity into the direction perpendicular to the net applied forces. When particles with a Magnus force term are driven perpendicular to the periodicity direction of a q1D periodic substrate, the Magnus term creates a coupling between the motion of the particles parallel and perpendicular to the driving force, so the effect of the q1D pinning becomes relevant. A Magnus term can arise for vortices in superconductors and superfluids; however, in the case of superconducting systems it is normally very small and has little effect on the depinning and sliding dynamics. Recently a new particle-like system, skyrmions in chiral magnets, was discovered in which the Magnus force is much stronger<sup>24-27</sup>. Since the initial observation of skyrmions in magnetic systems, there has been a rapid growth in the field as an increasing number of systems have been identified that support skyrmions, including materials in which skyrmions are stable at room temperature<sup>28-32</sup>. Another reason for the growing interest in this field is that skyrmions could be used as magnetic information carriers, making them promising for spintronic applications<sup>33</sup>.

In order for spintronic or other applications of skyrmions to be realized, it is necessary to have an understanding of how skyrmions move in different types of nanostructured samples. Skyrmions can be moved by an applied current<sup>27,34,35</sup>, and have been shown to exhibit a pinned to sliding transition based on effective velocity-force curves that can be constructed by mea-

sure changes in the transport properties<sup>36,37</sup>. Velocity-force curves can also be obtained by directly imaging the skyrmion motion<sup>27,28,38</sup>. In many cases the skyrmion critical depinning force is very low, and this was argued to be a result of the Magnus term which permits skyrmions to move around a pinning site and avoid trapping rather than moving toward the pinning site and becoming trapped as in the case of overdamped systems<sup>39-41</sup>. Under an applied driving force, the Magnus term causes the skyrmion to move at an angle with respect to the driving direction, producing a skyrmion Hall angle  $\theta_{sk}$ <sup>27,35,39</sup>. In a pin-free system  $\theta_{sk}$  is a constant and is proportional to the ratio of the Magnus term  $\alpha_m$  to the damping term  $\alpha_d$ ,  $\theta_{sk} \propto \tan^{-1}(\alpha_m/\alpha_d)$ . When pinning is present, however,  $\theta_{sk}$  becomes drive-dependent as the skyrmions make a side jump motion when interacting with an individual pinning site, which reduces the Hall angle<sup>41-43</sup>. As the drive is increased, the side jump effect is reduced and  $\theta_{sk}$  approaches the clean value limit. In Ref.<sup>44</sup> an imaging technique provided direct evidence for the drive dependence of the skyrmion Hall angle, with a linear dependence of the ratio of the transverse to longitudinal skyrmion velocity as a function of drive. These studies have focused on point-like pinning or circular pinning sites; however, it should also be possible to create line-like pinning using various lithographic techniques such as 1D periodic thickness modulation, periodic magnetic strips, or optical techniques.

In this work we use a particle-based simulation to examine individual and collectively interacting skyrmions in a 2D system in the presence of a q1D periodic substrate, as described Section II. The particle model is based on a modified Thiele equation<sup>40-43,45</sup> which agrees well with continuum-based simulations in the limit where the overlap of adjacent skyrmions is small<sup>40</sup>. In Section III we describe the results for the single skyrmion limit, where if the drive is applied parallel to the substrate periodicity direction, we find that unlike the case of point-like pinning, the depinning threshold does not decrease with increasing Magnus term magnitude since the skyrmions cannot simply move around the pinning sites. When the drive is applied perpendicular to the substrate periodicity direction, in the overdamped limit there is no depinning threshold and the skyrmions simply slide without any structural change for increasing drive, producing a linear velocity-force curve. On the other hand, when there is a finite Magnus term we observe a rich variety of dynamical behaviors even in the single skyrmion limit. For perpendicular drives, the skyrmion motion is locked in the drive direction at low drives until a critical driving force is reached at which the skyrmions also start move partially parallel to the substrate periodicity direction, coinciding with a sudden drop in the net velocity of the skyrmion and producing a negative differential conductivity effect. At higher drives the skyrmion velocity again increases with increasing drive. We also show that when the skyrmion motion is locked in the direction of the drive, a speed up effect occurs where the skyrmion

moves faster than it would in the overdamped limit due to the alignment of the pinning-induced velocity from the Magnus term with the driving force direction. This speed up effect was initially observed in simulations of point-like pinning<sup>41,42</sup>; however, the effect is more easily controlled with q1D pinning. When the driving is applied parallel to the substrate periodicity direction, there is no speed up effect but instead an enhanced damping appears. In Section IV we examine collectively interacting skyrmions and show that the same speed up effect and transition from locked motion in the direction of drive to motion in both the longitudinal and transverse directions occur. In addition, a series of dynamical phases appear that can be characterized by the structure of the moving skyrmions, and the transitions between these phases are correlated with distinct features in the transport curves. The phases include a moving smectic and a moving liquid which can undergo dynamical ordering transitions into a moving quasi-ordered hexatic lattice or a moving crystal. We map out the dynamic phases as a function of the substrate strength and the ratio of the Magnus force to the dissipative term. In Section V we examine the effect of changing the ratio of the skyrmion density to the periodicity of the substrate, where we observe chainlike structures consisting of multiple rows of skyrmions per substrate minimum. We also check for hysteresis across the dynamic phase transitions.

## II. SIMULATION

In Fig. 1 we show a snapshot of our 2D system, which has periodic boundary conditions in the  $x$  and  $y$  directions and contains a q1D periodic sinusoidal substrate potential with a period  $a$  and a periodicity running along the  $x$  direction. There are  $N$  skyrmions which are trapped in the potential minima. The initial skyrmion positions are obtained through simulated annealing, after which we apply a dc driving force  $\mathbf{F}^{dc}$  in either the parallel or  $x$  direction,  $\mathbf{F}^{dc} = F_{\parallel}^D \hat{\mathbf{x}}$ , or in the perpendicular or  $y$  direction,  $\mathbf{F}^{dc} = F_{\perp}^D \hat{\mathbf{y}}$ , and we measure the resulting skyrmion velocity. The dynamics of a single skyrmion  $i$  are obtained using the following equation of motion:

$$\alpha_d \mathbf{v}_i + \alpha_m \hat{\mathbf{z}} \times \mathbf{v}_i = \mathbf{F}_i^{ss} + \mathbf{F}_i^{sp} + \mathbf{F}^{dc} \quad (1)$$

where  $\mathbf{r}_i$  is the skyrmion position and  $\mathbf{v}_i = d\mathbf{r}_i/dt$  is the skyrmion velocity. The first term is the damping  $\alpha_d$  which aligns the skyrmion velocity in the direction of the net external forces, and the second term is the Magnus force with prefactor  $\alpha_m$ , where the cross product creates a velocity component perpendicular to the net external forces. To maintain a constant magnitude of the skyrmion velocity we apply the constraint  $\alpha_d^2 + \alpha_m^2 = 1$ . The skyrmion Hall effect can be characterized by measuring the ratio  $R = \langle V_{\perp} \rangle / \langle V_{\parallel} \rangle$  of the skyrmion velocity in the perpendicular direction,  $\langle V_{\perp} \rangle = N^{-1} \sum_i^N \mathbf{v}_i \cdot \hat{\mathbf{y}}$ , to

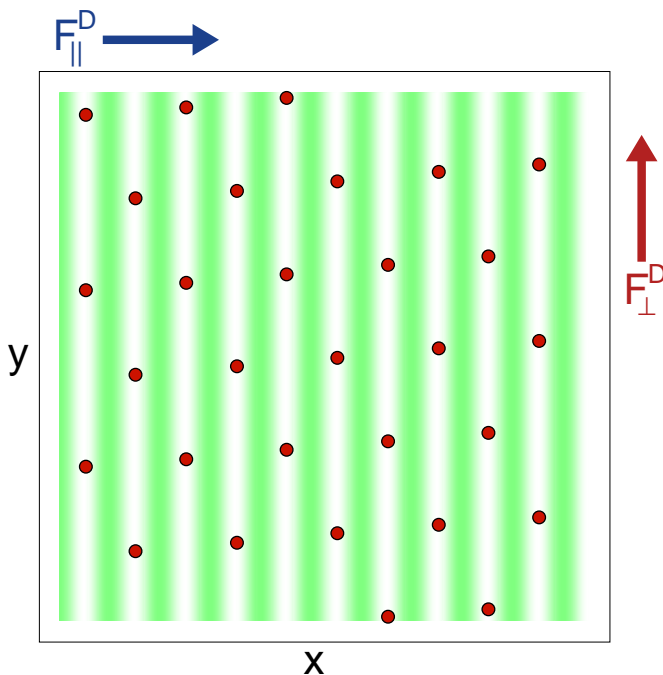


FIG. 1: (Color online) Skyrmions (red dots) at a density of  $\rho_s = 0.1$  on a periodic quasi-one-dimensional substrate with pinning strength  $A_p = 1.0$ . Here the substrate periodicity is in the  $x$ -direction and we consider dc driving  $F_{\parallel}^D$  in the parallel or  $x$  direction (blue arrow) and  $F_{\perp}^D$  in the perpendicular or  $y$  direction (red arrow). The dark green regions indicate the locations of the substrate potential maxima.

that in the parallel direction,  $\langle V_{\parallel} \rangle = N^{-1} \sum_i^N \mathbf{v}_i \cdot \hat{\mathbf{x}}$ . The skyrmion Hall angle is  $\theta_{sk} = \tan^{-1}(R)$ . In a clean system,  $R$  has a constant value given by  $R = \alpha_m/\alpha_d$ . The substrate force  $\mathbf{F}_i^{sp} = -\nabla U(x_i)\hat{\mathbf{x}}$  arises from a periodic sinusoidal potential

$$U(x_i) = U_0 \cos(2\pi x_i/a) \quad (2)$$

where  $x_i = \mathbf{r}_i \cdot \hat{\mathbf{x}}$ ,  $a$  is the periodicity of the substrate, and we define the substrate strength to be  $A_p = 2\pi U_0/a$ . The skyrmion-skyrmion interaction force is repulsive, which favors the formation of a triangular lattice in a clean system. It has the form  $\mathbf{F}_i^{ss} = \sum_{j=1}^N K_1(R_{ij})\hat{\mathbf{r}}_{ij}$  where  $R_{ij} = |\mathbf{r}_i - \mathbf{r}_j|$ ,  $\hat{\mathbf{r}}_{ij} = (\mathbf{r}_i - \mathbf{r}_j)/R_{ij}$ , and  $K_1$  is the modified Bessel function. This interaction falls off exponentially for large  $R_{ij}$ . The sample is of size  $L \times L$  and the skyrmion density is  $n_s = N/L^2$ . Previous studies of skyrmions on a similar q1D periodic substrate focused on Magnus-induced Shapiro steps, which arise when an additional ac drive is present<sup>1</sup>.

### III. SINGLE SKYRMION LIMIT

We first consider the case of a single skyrmion,  $N = 1$ . In Fig. 2(a) we plot  $\langle V_{\parallel} \rangle$  and  $\langle V_{\perp} \rangle$  versus  $F_{\parallel}^D$  for an

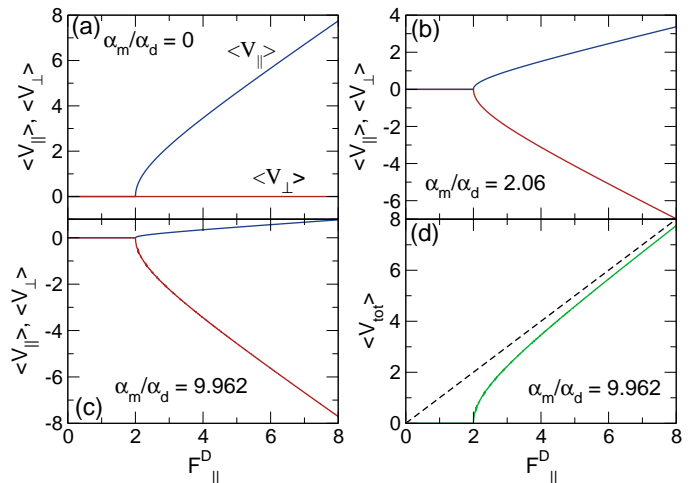


FIG. 2: (Color online) Parallel ( $\langle V_{\parallel} \rangle$ , blue) and perpendicular ( $\langle V_{\perp} \rangle$ , red) velocities for a single skyrmion driven in the parallel ( $x$ ) direction vs the driving force magnitude  $F_{\parallel}^D$ . The substrate potential strength is  $A_p = 2.0$ . (a) In the overdamped limit of  $\alpha_m/\alpha_d = 0$ , the motion is locked in the parallel direction and there is a critical depinning force of  $F_{\parallel}^c = 2.0$ . (b) At  $\alpha_m/\alpha_d = 2.06$ , there is a finite velocity signal in both directions. (c) At  $\alpha_m/\alpha_d = 9.962$ ,  $\langle V_{\parallel} \rangle$  is diminished compared to  $\langle V_{\perp} \rangle$ . (d)  $\langle V_{\text{tot}} \rangle = \sqrt{\langle V_{\parallel} \rangle^2 + \langle V_{\perp} \rangle^2}$  vs  $F_{\parallel}^D$  for  $\alpha_m/\alpha_d = 9.962$ . The dashed line indicates the response  $\langle V_{\text{tot}}^0 \rangle$  for a clean system with  $A_p = 0$ . The  $\langle V_{\text{tot}}^0 \rangle$  curve does not vary as a function of  $\alpha_m/\alpha_d$ .

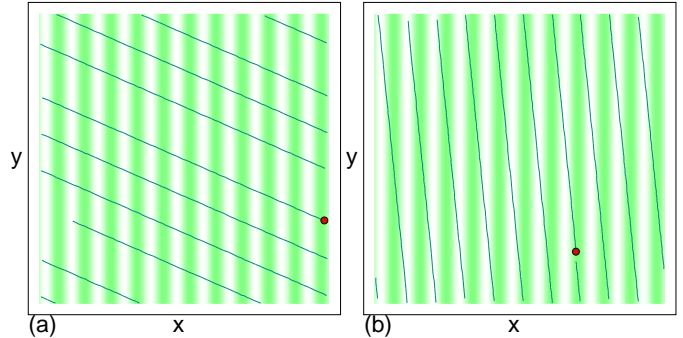


FIG. 3: The skyrmion location (red circle), trajectory (line), and substrate potential (green) for the system in Fig. 2 just above depinning. The dc drive  $F_{\parallel}^D$  is in the positive  $x$ -direction. (a) At  $\alpha_m/\alpha_d = 0.4364$ , the skyrmion moves at an angle of  $\theta_{sk} = 23.6^\circ$  with respect to the driving direction. (b) At  $\alpha_m/\alpha_d = 9.9624$ ,  $\theta_{sk} = 84.26^\circ$ .

overdamped system with  $\alpha_m/\alpha_d = 0$  where the particle is driven parallel to the substrate periodicity direction and the substrate strength is  $A_p = 2.0$ . Here,  $\langle V_{\perp} \rangle = 0$  for all  $F_{\parallel}^D$ , and there is a depinning transition at  $F_{\parallel}^c = A_p = 2.0$ , above which  $\langle V_{\parallel} \rangle$  becomes finite. Figure 2(b) shows that at  $\alpha_m/\alpha_d = 2.06$ , the depinning threshold is still  $F_{\parallel}^c = 2.0$ , but the skyrmion now moves both parallel and perpendicular to the driv-

ing direction above depinning. The slope of the  $\langle V_{\perp} \rangle$  curve is approximately twice that of the  $\langle V_{\parallel} \rangle$  curve. At  $\alpha_m/\alpha_d = 9.962$ , Fig. 2(c) shows that the depinning threshold is unchanged at  $F_{\parallel}^c = 2.0$  but that the perpendicular velocity has become much more pronounced. We find that  $F_{\parallel}^c$  is independent of  $\alpha_m/\alpha_d$  for driving in the parallel direction. This is in contrast to observations of skyrmions interacting with randomly placed<sup>39,40,43</sup> or periodic<sup>41</sup> arrays of pointlike pinning sites, where  $F_{\parallel}^c$  decreases with increasing  $\alpha_m/\alpha_d$ . For pointlike pinning, as the increasing Magnus term causes the skyrmion trajectories to become increasingly curved, the skyrmions can more easily circle around the pinning sites without becoming trapped, and this has been argued to be one of the reasons that the depinning thresholds are so low in skyrmion systems. In the case of the q1D periodic substrate, the pinning potential is planar in one direction, making it impossible for the skyrmions to circle around the pinning locations. As a result, planar or linelike pinning sites produce much stronger skyrmion pinning than pointlike pinning sites.

In Fig. 2(d) we plot the total velocity  $\langle V_{\text{tot}} \rangle = \sqrt{\langle V_{\parallel} \rangle^2 + \langle V_{\perp} \rangle^2}$  for the system in Fig. 2(c) with  $\alpha_m/\alpha_d = 9.962$ . The dashed line indicates the response  $\langle V_{\text{tot}}^0 \rangle$  in a clean system with  $A_p = 0$  for comparison. Here, for any finite value of  $A_p$ ,  $\langle V_{\text{tot}} \rangle < \langle V_{\text{tot}}^0 \rangle$  for parallel driving, indicating that the effective damping is enhanced by the substrate. In Fig. 3(a) we plot the skyrmion trajectory just above depinning for the system in Fig. 2 at  $\alpha_m/\alpha_d = 0.4364$ . The skyrmion follows a straight trajectory oriented at an angle, the skyrmion Hall angle  $\theta_{sk} = 23.6^\circ$ , with respect to the external drive. Figure 3(b) shows that at  $\alpha_m/\alpha_d = 9.9624$ , the skyrmion moves at a much steeper angle to the external drive, with  $\theta_{sk}$  just under the clean limit value of  $\theta_{sk} = 84.26^\circ$ .

In Fig. 4 we show  $\langle V_{\perp} \rangle$  and  $\langle V_{\parallel} \rangle$  versus  $F_{\perp}^D$  for a single skyrmion driven along the  $y$  direction, perpendicular to the substrate symmetry direction. In the overdamped limit of  $\alpha_m/\alpha_d = 0$ ,  $\langle V_{\parallel} \rangle = 0$  for all  $F_{\perp}^D$ , there is no depinning threshold for motion in the driving direction, and  $\langle V_{\perp} \rangle$  increases linearly with  $F_{\perp}^D$ . When  $\alpha_m/\alpha_d > 0$ , there is a range of  $F_{\perp}^D$  over which the skyrmion motion is locked in the perpendicular or  $y$  direction, and once  $F_{\perp}^D$  reaches a critical threshold  $F_{\perp}^c$ , a transition occurs to motion in both the perpendicular and parallel directions. This is illustrated in Fig. 4(a) for  $\alpha_m/\alpha_d = 0.577$ , where  $\langle V_{\parallel} \rangle$  becomes finite at  $F_{\perp}^D = F_{\perp}^c = 3.5$ . This transition coincides with a small drop in  $\langle V_{\perp} \rangle$ . As  $\alpha_m/\alpha_d$  is increased, the value of  $F_{\perp}^c$  decreases while the magnitude of the drop in  $\langle V_{\perp} \rangle$  at the transition point increases, as shown in Fig. 4(b,c) for  $\alpha_m/\alpha_d = 2.06$  and  $9.962$ , respectively. For  $F_{\perp}^D > F_{\perp}^c$ ,  $\langle V_{\perp} \rangle$  increases with increasing  $F_{\perp}^D$ . In Fig. 5(a) we plot the skyrmion trajectory for the system in Fig. 4(c,d) with  $\alpha_m/\alpha_d = 9.962$  at  $F_{\perp}^D = 0.17$ , where the skyrmion motion is locked in the drive direction. At  $F_{\perp}^D = 0.6$  in Fig. 5(b), the skyrmion moves in both the longitudinal and transverse directions with a sinusoidal undulation. In Fig. 5(c) at  $F_{\perp}^D = 1.0$ , the an-

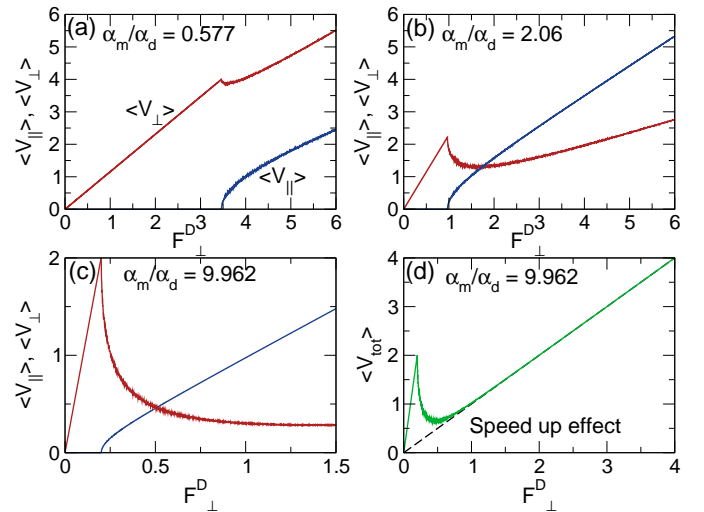


FIG. 4:  $\langle V_{\parallel} \rangle$  and  $\langle V_{\perp} \rangle$  for a single skyrmion driven in the perpendicular ( $y$ ) direction vs the driving force magnitude  $F_{\perp}^D$ . The substrate potential strength is  $A_p = 2.0$ . (a) At  $\alpha_m/\alpha_d = 0.577$ , the skyrmion motion is initially locked in the perpendicular direction, and a transition to motion in both the parallel and perpendicular directions occurs at  $F_{\perp}^c = 3.5$ . (b) At  $\alpha_m/\alpha_d = 2.06$ ,  $F_{\perp}^c$  is decreased. (c) At  $\alpha_m/\alpha_d = 9.962$ ,  $F_{\perp}^c$  is even smaller. (d)  $\langle V_{\text{tot}} \rangle$  vs  $F_{\perp}^D$ , where the dashed line indicates the response  $\langle V_{\text{tot}}^0 \rangle$  in a system with  $A_p = 0$ . Here  $\langle V_{\text{tot}} \rangle > \langle V_{\text{tot}}^0 \rangle$ , indicating the existence of a speed up effect.

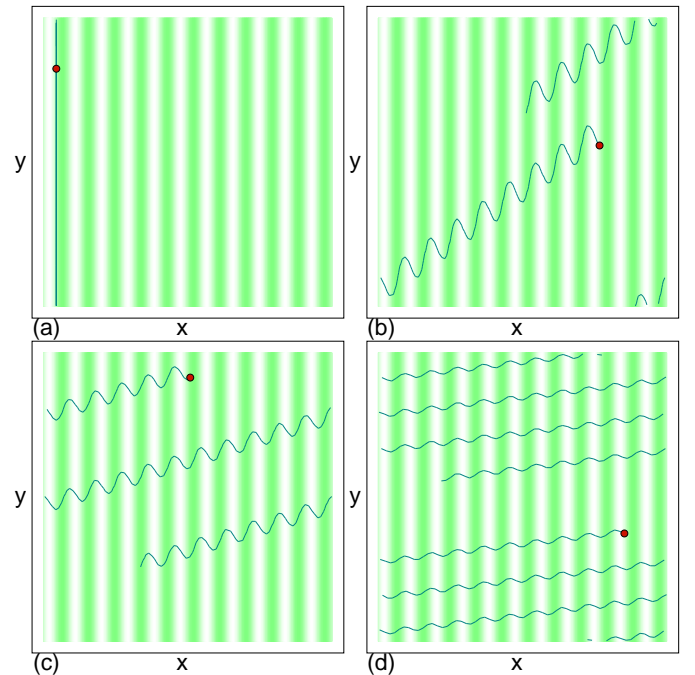


FIG. 5: The skyrmion location (red circle), trajectory (line), and substrate potential (green) for the system in Fig. 4(c,d) at  $\alpha_m/\alpha_d = 9.962$ . The dc drive  $F_{\perp}^D$  is in the positive  $y$ -direction. (a) At  $F_{\perp}^D = 0.17$ , the motion is locked in the driving direction. (b) At  $F_{\perp}^D = 0.6$ , the skyrmion moves at an angle with respect to the dc drive. (c)  $F_{\perp}^D = 1.0$ . (d)  $F_{\perp}^D = 3.0$ .

gle  $\theta_{sk}$  between the direction of skyrmion motion and the driving direction is larger, while at  $F_{\perp}^D = 3.0$  in Fig. 5(d),  $\theta_{sk}$  is even larger. For high enough drives,  $\theta_{sk}$  approaches the clean limit value of  $\theta_{sk} = 84.26^\circ$ . This shows that the skyrmion Hall angle has a much stronger dependence on the external driving force for perpendicular driving than for parallel driving.

In Fig. 4(d) we plot the net velocity  $\langle V_{\text{tot}} \rangle$  versus  $F_{\perp}^D$  at  $\alpha_m/\alpha_d = 9.962$ . The dashed line shows the response  $\langle V_{\text{tot}}^0 \rangle$  for a system with  $A_p = 0$ . Just above the depinning threshold  $F_{\perp}^c = 0.2$  for motion in the parallel direction, we observe negative differential conductivity (NDC), where the net velocity of the skyrmion decreases with increasing drive. Negative differential conductivity is a phenomenon often found for charge transport in semiconductors<sup>46</sup>, and it can be useful in constructing logic devices, which suggests that the construction of magnetic versions of semiconductor logic devices using skyrmions may be possible. NDC has also been observed for vortices in type-II superconductors driven over periodic pinning arrays, where it is associated with transitions in the flow states<sup>18,20</sup>. Previous simulation studies of skyrmions driven over 2D periodic arrays, where the skyrmion Hall angle changes as a function of drive, also showed NDC<sup>41</sup>, while in both particle-based and continuum simulations of skyrmions interacting with an isolated circular pinning site, the skyrmion velocity can drop to zero at high enough drive when it becomes possible for the pinning site to capture a skyrmion<sup>42</sup>.

Figure 4(d) also shows that  $\langle V_{\text{tot}} \rangle$  is always larger than the clean limit value of  $\langle V_{\text{tot}}^0 \rangle$ , indicating that the q1D substrate enhances the skyrmion velocity compared to the clean limit. For example, at the parallel depinning transition point  $F_{\perp}^D = F_{\perp}^c = 0.2$ ,  $\langle V_{\text{tot}} \rangle \approx 2.0$ , while in the pin-free limit,  $\langle V_{\text{tot}}^0 \rangle = F_{\perp}^D = 0.2$ . Such speed up effects were first observed in continuum and particle based simulations for skyrmions interacting with a single pinning site<sup>42</sup> and with a periodic array of pinning sites<sup>41</sup>. In the case of q1D planar pinning sites, it is easier to see that this effect arises due to the Magnus force. Due to the damping term, the perpendicular external drive  $F_{\perp}^D$  produces a perpendicular velocity component of  $\langle V_{\perp}^d \rangle = \alpha_d F_{\perp}^D$ . The Magnus term transfers some of the motion produced by the drive into the parallel direction, giving a finite value of  $\langle V_{\parallel} \rangle$ ; however, the pinning imparts a force proportional to  $A_p$  on the skyrmion in the parallel direction. This parallel force is transformed by the Magnus term into a perpendicular velocity, leading to an additional velocity contribution of  $\langle V_{\perp}^m \rangle = \alpha_m A_p$ . As long as the skyrmion motion remains locked in the perpendicular direction, its maximum perpendicular velocity is given by

$$\langle V_{\perp}^{\text{max}} \rangle = \alpha_d F_{\perp}^c + \alpha_m A_p. \quad (3)$$

In Fig. 4(c,d) we use  $\alpha_d = 0.09987$  and  $\alpha_m = 0.995$ , so that at the transition point  $F_{\perp}^D = 0.2$  we obtain  $\langle V_{\perp}^{\text{max}} \rangle = 2.001$ , in agreement with the maximum values of  $\langle V_{\perp} \rangle$  and  $\langle V_{\text{tot}} \rangle$  in Fig. 4(c,d). This shows that the

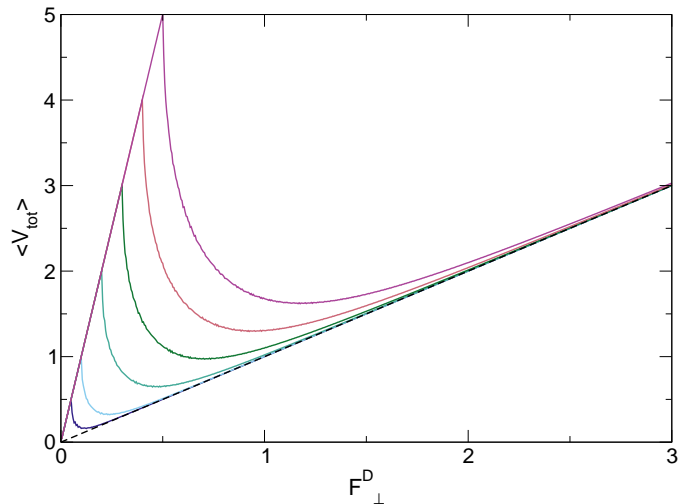


FIG. 6:  $\langle V_{\text{tot}} \rangle$  vs  $F_{\perp}^D$  at  $\alpha_m/\alpha_d = 9.962$  for  $A_p = 0.5, 1.0, 2.0, 3.0, 4.0, 5.0$ , from bottom to top. The dashed line is  $\langle V_{\text{tot}}^0 \rangle$  with  $A_p = 0$ .

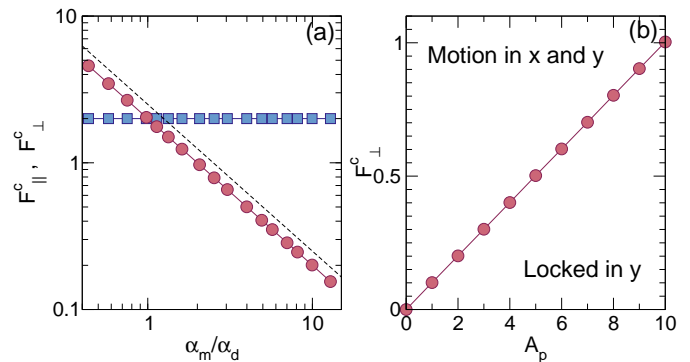


FIG. 7: (a) The depinning forces  $F_{\parallel}^c$  and  $F_{\perp}^c$  at which motion in the direction parallel to the substrate periodicity occurs vs  $\alpha_m/\alpha_d$  for samples with  $A_p = 2.0$ . Blue squares:  $F_{\parallel}^c$ , for parallel driving, has no dependence on  $\alpha_m/\alpha_d$ . Red circles:  $F_{\perp}^c$ , for perpendicular driving, can be fit to  $F_{\perp}^c \propto (\alpha_m/\alpha_d)^{-1}$  (dashed line). (b)  $F_{\perp}^c$  vs  $A_p$  at  $\alpha_m/\alpha_d = 9.962$ . Here  $F_{\perp}^c$  increases linearly with  $A_p$ .

skyrmion velocity can increase linearly with the pinning force. Once the system depins in the parallel direction at  $F_{\perp}^c$ , the skyrmion experiences an oscillating pinning force, causing the speed up effect to be lost and  $\langle V_{\perp} \rangle$  to drop. At high drives the system gradually approaches the clean value limit in which the velocity increases linearly with drive according to  $\langle V_{\perp} \rangle = \alpha_d F_{\perp}^D$  and  $\langle V_{\parallel} \rangle = \alpha_m F_{\perp}^D$ , as also observed in systems with periodic and random pointlike pinning<sup>43</sup>. In Fig. 6 we plot  $\langle V_{\text{tot}} \rangle$  versus  $F_{\perp}^D$  for  $A_p = 0.5, 1.0, 2.0, 3.0, 4.0, 5.0$  at  $\alpha_m/\alpha_d = 9.962$ . Here, both  $F_{\perp}^c$  and the maximum value of  $\langle V_{\text{tot}} \rangle$  increase with  $A_p$ , in agreement with Eq. 3.

In Fig. 7(a) we plot the depinning force  $F_{\parallel}^c$  versus  $\alpha_m/\alpha_d$  for parallel driving for the system in Fig. 2 along with the force  $F_{\perp}^c$  at which sliding along the parallel di-



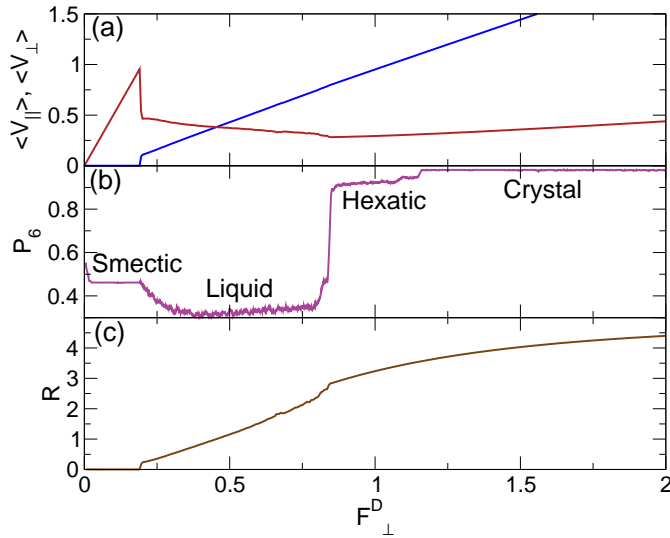


FIG. 8: (a)  $\langle V_{\parallel} \rangle$  (blue) and  $\langle V_{\perp} \rangle$  (red) vs  $F_{\perp}^D$  for a system with multiple interacting skyrmions at  $\alpha_m/\alpha_d = 4.925$ ,  $A_p = 1.0$ , and skyrmion density  $n_s = 0.16$ . (b) The fraction of sixfold-coordinated skyrmions  $P_6$  vs  $F_{\perp}^D$ . In the moving smectic phase the motion is locked along the perpendicular direction. Also marked are the moving liquid, moving hexatic, and moving crystal phases. (c)  $R = \langle V_{\perp} \rangle / \langle V_{\parallel} \rangle$  vs  $F_{\perp}^D$ .

rection occurs for the system in Fig. 4 with perpendicular driving.  $F_{\parallel}^c$  is constant and  $F_{\perp}^c$  obeys  $F_{\perp}^c \propto (\alpha_m/\alpha_d)^{-1}$ , as indicated by the dashed line, so that  $F_{\perp}^c$  diverges at  $\alpha_m = 0$  when the skyrmions stay locked in the direction of drive in the overdamped limit. Figure 7(b) shows  $F_{\perp}^c$  versus  $A_p$  for  $\alpha_m/\alpha_d = 9.962$ , showing a linear increase with  $A_p$  with a slope of  $A_p/\alpha_m$ .

#### IV. COLLECTIVE EFFECTS

We next consider the case of multiple interacting skyrmions. In Fig. 8(a) we plot  $\langle V_{\parallel} \rangle$  and  $\langle V_{\perp} \rangle$  versus  $F_{\perp}^D$  for a system with  $\alpha_m/\alpha_d = 4.925$  and  $A_p = 1.0$  at a skyrmion density of  $n_s = 0.16$ , where the ratio of the substrate lattice constant  $a$  to the skyrmion lattice constant  $a_{sk}$  is  $a/a_{sk} = 1.3098$ . Here we observe the same features in  $\langle V_{\parallel} \rangle$  and  $\langle V_{\perp} \rangle$  that appeared in the single skyrmion case, including a longitudinally locked phase, negative differential conductivity, and a speed up effect. There are several differences, including additional cusps in the velocity-force curves at higher drives which are correlated with changes in the collective dynamics. Fig. 8(b) shows  $P_6$ , the fraction of sixfold-coordinated skyrmions, versus  $F_{\perp}^D$ . Here  $P_6 = N^{-1} \sum_{i=1}^N \delta(z_i - 6)$ , where  $z_i$  is the coordination number of skyrmion  $i$  obtained from a Voronoi construction. In the longitudinally locked regime, the pinning is strong enough that the skyrmions form 1D incommensurate chains moving in the perpendicular direction, so that the skyrmion lattice structure exhibits a number of aligned topological defects. Figure 9(a) shows

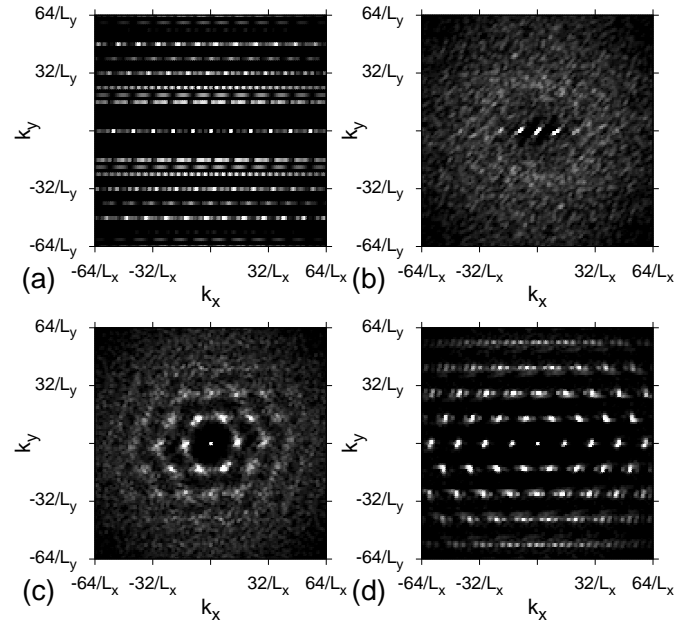


FIG. 9: The structure factor  $S(\mathbf{k})$  for the different phases for the system in Fig. 8. (a) The moving smectic phase at  $F_{\perp}^D = 0.1$ . (b) The moving liquid phase at  $F_{\perp}^D = 0.5$ . (c) The moving hexatic phase at  $F_{\perp}^D = 1.0$ . (d) The moving crystal phase at  $F_{\perp}^D = 1.2$ .

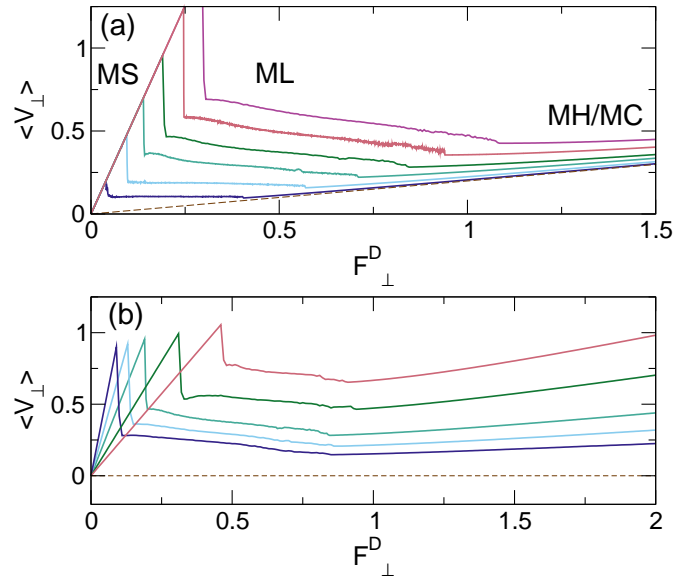


FIG. 10: (a)  $\langle V_{\perp} \rangle$  vs  $F_{\perp}^D$  for the system in Fig. 8 at  $\alpha_m/\alpha_d = 4.925$  for  $A_p = 0.25, 0.5, 0.75, 1.0, 1.25, 1.5$ , from bottom to top, showing more clearly the cusp at the ML-MH/MC transition. MS: moving smectic; ML: moving liquid; MH: moving hexatic; MC: moving crystal. The dashed line is the response for a sample with  $A_p = 0$ . (b)  $\langle V_{\perp} \rangle$  vs  $F_{\perp}^D$  for the same system with  $A_p = 1.0$  for  $\alpha_m/\alpha_d = 9.995, 7.017, 4.925, 3.0, 2.06$ , from top right to bottom right. The dashed line indicates the response in an overdamped system with  $\alpha_m/\alpha_d = 0$ .

the structure factor  $S(\mathbf{k}) = N^{-1} |\sum_i^N \exp(-i\mathbf{k} \cdot \mathbf{r}_i)|^2$  for the moving smectic (MS) phase at  $F_{\perp}^D = 0.1$ , where the system forms stripe like features indicative of smectic ordering. For  $0.18 < F_{\perp}^D < 0.84$ ,  $\langle V_{\perp} \rangle$  gradually decreases with increasing  $F_{\perp}^D$  and the skyrmions form a disordered or moving liquid (ML) state, as indicated by the ring structure in Fig. 9(b), which shows  $S(\mathbf{k})$  at  $F_{\perp}^D = 0.5$ . There are still two satellite peaks in  $S(\mathbf{k})$  along the  $k_y = 0$  line that are produced by the 1D periodicity of the substrate.

In Fig. 8, a cusp appears in  $\langle V_{\perp} \rangle$  near  $F_{\perp}^D = 0.85$ , above which  $\langle V_{\perp} \rangle$  starts to increase with increasing  $F_{\perp}^D$  again. This cusp is correlated with a sharp increase in  $P_6$  to  $P_6 = 0.93$ , which indicates that the system has dynamically reordered into a triangular lattice containing a small number of fivefold and sevenfold-coordinated defects. We call this a moving hexatic (MH) state, and it exhibits smeared sixfold peaks in  $S(\mathbf{k})$ , as shown in Fig. 9(c) at  $F_{\perp}^D = 1.0$ . Near  $F_{\perp}^D = 1.16$ , there is another jump in  $P_6$  to  $P_6 \approx 1.0$ . Here the system forms a moving crystal (MC) phase, and the corresponding structure factor in Fig. 9(d) shows much more pronounced peaks in  $S(\mathbf{k})$ . In Fig. 8(c) we plot the velocity ratio  $R$  versus  $F_{\perp}^D$ . There is a jump to a finite value of  $R$  at the onset of the ML phase, and a cusp at the ML-MH transition. We do not observe any particular cusps or jumps in the transport curves at the MH-MC transition. In Fig. 10(a) we plot  $\langle V_{\perp} \rangle$  versus  $F_{\perp}^D$  for the system in Fig. 8 for  $A_p = 0.25, 0.5, 0.75, 1.0, 1.25$ , and  $1.5$ , with a dashed line indicating the response for  $A_p = 0$ . Here the cusp in  $\langle V_{\perp} \rangle$  at the ML-MH/MC transition can be more clearly seen. Additionally, the velocity noise fluctuations are substantially reduced in the dynamically ordered MH/MC states. In Fig. 10(b) we show  $\langle V_{\perp} \rangle$  versus  $F_{\perp}^D$  for samples with  $A_p = 1.0$  at  $\alpha_m/\alpha_d = 9.995, 7.017, 4.925, 3.0$ , and  $2.06$ . The MS-ML transition shifts to higher values of  $F_{\perp}^D$  with decreasing  $\alpha_m/\alpha_d$ , while the cusps at higher  $F_{\perp}^D$  indicate the ML-MH/MC transition is still present.

The onset of different dynamical phases as a function of external driving has been observed in various overdamped systems, including colloids and vortices moving over q1D periodic substrates, but only for a driving force applied parallel to the substrate periodicity direction. In those systems there is generally a disordered flow phase above depinning<sup>7,14,47,48</sup> with a transition to a moving ordered phase at higher drives<sup>14,47,48</sup>; however, negative differential conductivity does not occur. For systems of particles moving over 2D periodic substrates, such as egg carton or muffin tin potentials, negative differential conductivity can arise<sup>18,20,49–51</sup>. In previous simulations of skyrmions driven over random arrays, it was shown that there can be a transition from a disordered phase above depinning to a moving crystal phase at higher drive<sup>43</sup>, while there are extensive studies of dynamically ordered phases as a function of increasing driving force for vortices driven over random pinning arrays<sup>52–55</sup>.

We have also considered the case of interacting

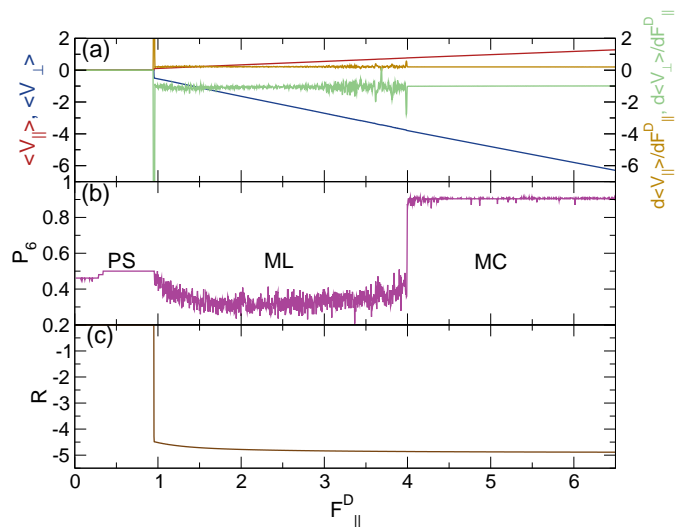


FIG. 11: The same system as in Fig. 8 but for driving parallel to the substrate periodicity direction. (a)  $\langle V_{\parallel} \rangle$  (red) and  $\langle V_{\perp} \rangle$  (blue) vs  $F_{\parallel}^D$ , along with the corresponding  $d\langle V_{\parallel} \rangle/dF_{\parallel}^D$  (yellow) and  $d\langle V_{\perp} \rangle/dF_{\parallel}^D$  (green) curves. (b)  $P_6$  vs  $F_{\parallel}^D$  showing transitions between the pinned smectic (PS) state, the moving liquid (ML), and the moving crystal (MC). (c) Velocity ratio  $R$  vs  $F_{\parallel}^D$ .

skyrmions subjected to a drive that is applied parallel to the substrate periodicity. In Fig. 11(a) we plot  $\langle V_{\parallel} \rangle$  and  $\langle V_{\perp} \rangle$  versus  $F_{\parallel}^D$  for a system with  $\alpha_m/\alpha_d = 4.925$ ,  $A_p = 1.0$ , and  $n_s = 0.16$ . Here the depinning threshold  $F_{\parallel}^c \approx A_p$ , and in general for fixed  $n_s$ ,  $F_{\parallel}^c$  is independent of  $\alpha_m/\alpha_d$  and increases linearly with  $A_p$ , similar to the results for the single skyrmion case shown in Fig. 2. The interacting skyrmions form an immobile pinned smectic (PS) phase which depins plastically into a moving liquid (ML) state. The ML dynamically orders into a moving crystal (MC) phase near  $F_{\parallel}^D = 4.0$ , as is illustrated by the plot of  $P_6$  versus  $F_{\parallel}^D$  in Fig. 11(b). There is only a small cusp in the transport curves at the ML-MC transition, as indicated by the  $d\langle V_{\parallel} \rangle/dF_{\parallel}^D$  and  $d\langle V_{\perp} \rangle/dF_{\parallel}^D$  plots in Fig. 11(a). This contrasts with the significantly larger cusps that appear for perpendicular driving. Additionally, the velocity fluctuations are strongly suppressed once the system enters the MC phase. The MC phase that forms for parallel driving generally contains more dislocations than the corresponding MC phase that appears for perpendicular driving, so the parallel driving MC phase can better be described as a moving hexatic. In Fig. 11(c), the plot of the velocity ratio  $R$  versus  $F_{\parallel}^D$  shows that the PS-ML transition is sharp. There is little curvature in  $R$  for higher drives, in contrast to the perpendicular driving case where  $R$  increases much more smoothly as a function of drive.

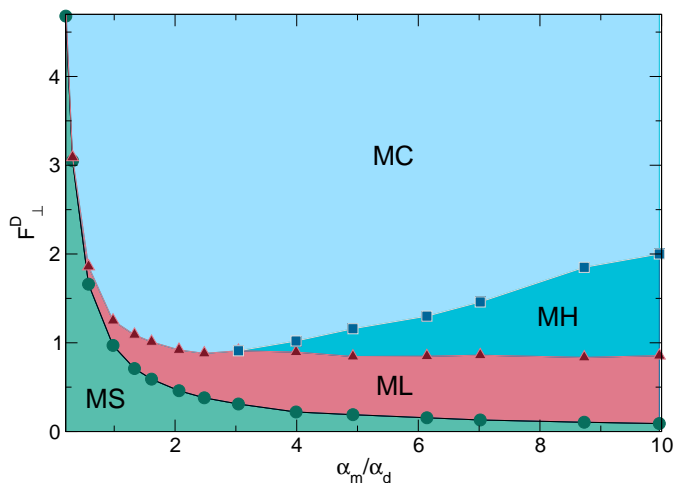


FIG. 12: The dynamic phase diagram as a function of  $F_{\perp}^D$  vs  $\alpha_m/\alpha_d$  for  $A_p = 1.0$  and  $n_s = 1.0$  showing the moving smectic (MS), moving liquid (ML), moving hexatic (MH), and moving crystal (MC) phases. Here the width of the MS phase diverges with decreasing  $\alpha_m/\alpha_d$ .

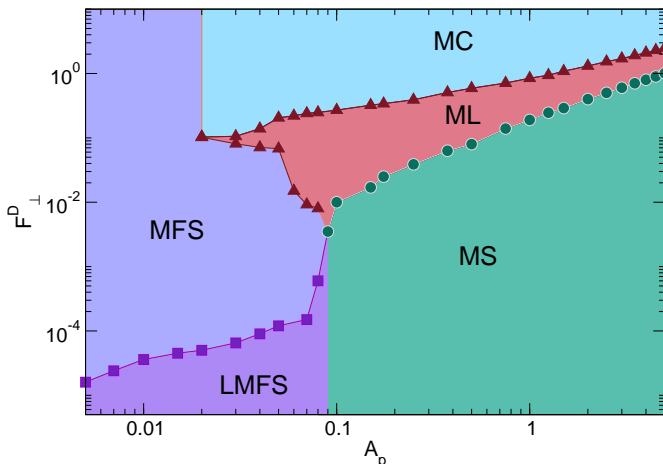


FIG. 13: The dynamic phase diagram as a function of  $F_{\perp}^D$  vs  $A_p$  at  $\alpha_m/\alpha_d = 4.925$  and  $n_s = 1.0$  showing the moving solid (MS), moving liquid (ML), and moving crystal (MC) phases. For weaker substrate strengths, a longitudinally locked moving floating solid (LMFS) phase appears which transitions with increasing  $F_{\perp}^D$  into a phase called the moving floating solid (MFS) that moves in both the parallel and perpendicular directions.

### A. Dynamic Phase Diagrams

By conducting a series of simulations and examining the features in  $\langle V_{\perp} \rangle$  and  $P_6$ , we can map out the dynamic phases, as shown in Fig. 12 as a function of  $F_{\perp}^D$  versus  $\alpha_m/\alpha_d$  for a system with  $A_p = 1.0$ . The extent of the MS phase diverges at small  $\alpha_m/\alpha_d$ , while the extent of the ML phase decreases with decreasing  $\alpha_m/\alpha_d$ . Based on features in the  $P_6$  curves, we find that the MH phase appears only for  $\alpha_m/\alpha_d > 3.0$ , and that it grows

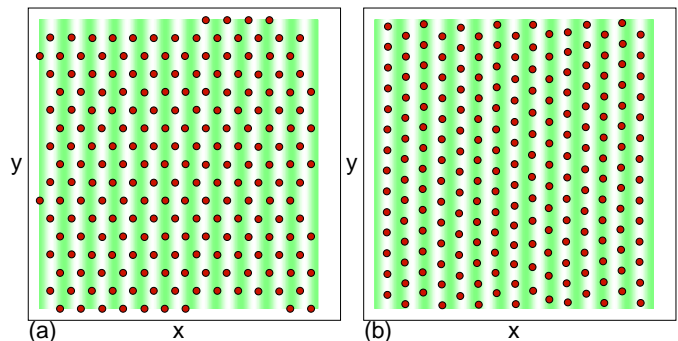


FIG. 14: (a) Image of skyrmion locations (red dots) on the substrate potential (green) for the system in Fig. 13 in the moving floating solid (MFS) state at  $A_p = 0.04$  and  $F_{\perp}^D = 0.0001$ . (b) The same for the moving crystal (MC) at  $F_{\perp}^D = 1.0$ , showing the change in the orientation of the lattice. The LMFS state has the same orientation as the MFS state.

in extent with increasing  $\alpha_m/\alpha_d$ . We have also considered the case of varied  $A_p$ , and in Fig. 13 we plot the dynamic phase diagram for  $F_{\perp}^D$  versus  $A_p$  for a system with  $\alpha_m/\alpha_d = 4.925$ . Here, the extent of the MS phase increases with increasing  $A_p$ , and the onset of the MC phase shifts to higher  $F_{\perp}^D$ . There is also a thin strip of MH phase that appears for  $A_p > 0.1$  (not shown). For weak enough  $A_p$ , additional dynamical phases appear when the skyrmions do not remain confined to the potential minima but form a completely triangular lattice that is weakly coupled to the substrate. At low  $F_{\perp}^D$ , the system forms a MS phase for  $A_p \geq 0.1$ , while for  $A_p < 0.1$  we observe a moving longitudinally locked floating solid (LMFS) which travels strictly along the perpendicular direction. Here, the skyrmions are pinned by the substrate in the parallel direction but can move freely along the perpendicular direction. At higher drives the LMFS transitions to a moving floating solid (MFS) phase in which the skyrmions depin from the weak substrate and begin to move in both the parallel and perpendicular directions.

Figure 13 shows that the value of  $F_{\perp}^D$  at which the system depins in the parallel direction and ceases to have its motion locked along the perpendicular direction drops substantially from the MS to the LMFS phase. This is similar to what is observed at an Aubry transition which arises in a 1D incommensurate Frenkel-Kontorova system, where when the substrate is weak enough, the pinning effectively vanishes and the particles float over the substrate<sup>56</sup>. It has been argued that an Aubry-like transition should occur for 2D systems such as sliding colloids<sup>57</sup>, and that this transition could be relevant to the phenomenon called superlubricity<sup>22</sup>. In recent simulations of colloids on 2D substrates, it was shown that the 2D Aubry transition is first order and is associated with a sharp drop in the effective friction<sup>57</sup>. This is similar to what we observe, where there is a sharp drop in the parallel depinning force at the MS-LMFS transition, suggesting that this transition is first order.



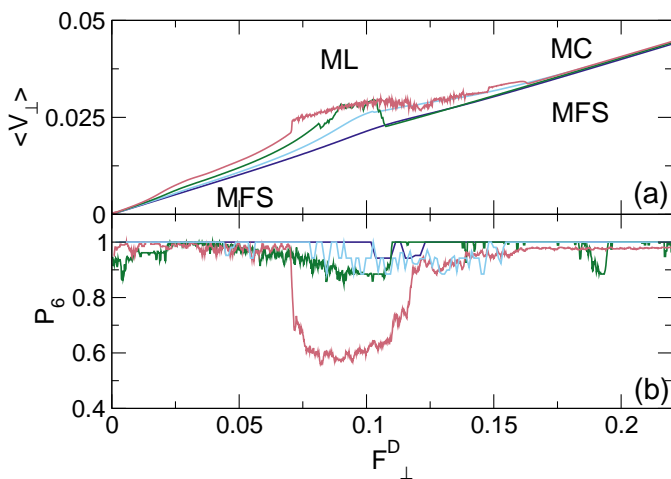


FIG. 15:  $\langle V_{\perp} \rangle$  vs  $F_{\perp}^D$  for the system in Fig. 13 at  $A_p = 0.01$  (dark blue), 0.02 (light blue), 0.03 (green), and 0.04 (pink). (b) The corresponding  $P_6$  vs  $F_{\perp}^D$  showing that at  $A_p = 0.01$  the system remains ordered, while at  $A_p = 0.04$ , the system goes from an ordered state into a disordered state and then dynamically orders at higher drives.

There is a window of  $A_p$  in the phase diagram of Fig. 13 in which the MFS can transition to a ML phase, which then dynamically orders into an MC phase at higher drives, while for low enough  $A_p$ , the ML phase is lost and no structural changes occur in the moving skyrmion lattice as a function of  $F_{\perp}^D$ . The orientation of the skyrmion lattice with respect to the substrate periodicity direction is generally different in the MC and the MFS phases. In the MC, the lattice is aligned with the substrate minima, while in the MFS there is no particular matching between the lattice orientation and the substrate periodicity direction, as shown in the images in Fig. 14(a,b) at  $A_p = 0.04$  for  $F_{\perp}^D = 0.0001$  and  $F_{\perp}^D = 1.0$ . In Fig. 15(a) we plot  $\langle V_{\perp} \rangle$  versus  $F_{\perp}^D$  curves from the phase diagram in Fig. 13 for  $A_p = 0.01, 0.02, 0.03$ , and 0.04. At  $A_p = 0.01$ ,  $\langle V_{\perp} \rangle$  is smooth, and no change occurs in the structure of the moving triangular lattice, while for  $A_p = 0.02$ , there is the beginning of a cusp feature at  $F_{\perp}^D = 0.1$ . For  $A_p = 0.03$ , a larger cusp appears that is associated with the system entering the ML phase, and a sharp drop in  $\langle V_{\perp} \rangle$  occurs when the system transitions to the moving crystal phase. The extent of the ML phase increases for higher values of  $A_p$ , as shown by the curve for  $A_p = 0.04$ . In Fig. 15(b), the corresponding  $P_6$  versus  $F_{\perp}^D$  curves indicate that at  $A_p = 0.01$ , the skyrmion lattice remains triangular with  $P_6 = 1.0$  over nearly the entire range of  $F_{\perp}^D$ . In contrast, for  $A_p = 0.04$  the system transitions from a low drive moving ordered state with  $P_6 \approx 1.0$  into the ML liquid state, as shown by the drop to  $P_6 \approx 0.6$ . This is followed at higher drives by a transition into the moving crystal phase where  $P_6 \approx 1.0$  again.

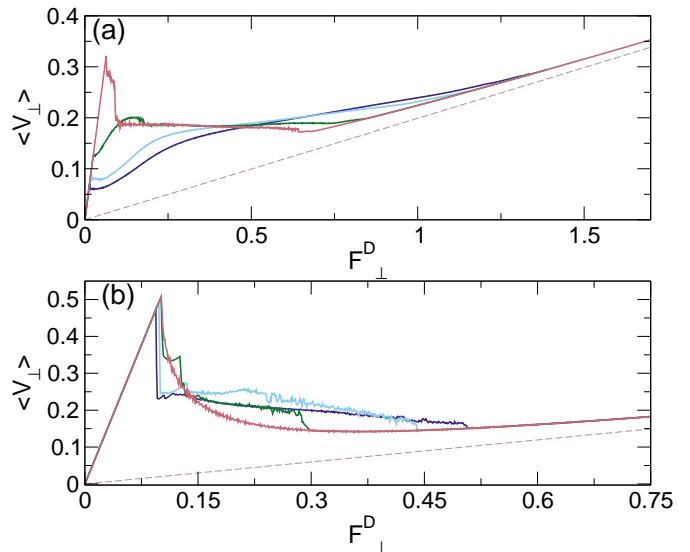


FIG. 16:  $\langle V_{\perp} \rangle$  vs  $F_{\perp}^D$  for samples with  $\alpha_m/\alpha_d = 4.925$  and  $A_p = 0.5$  at varied skyrmion densities  $n_s$ . (a)  $n_s = 0.44$  (dark blue), 0.36 (light blue), 0.262 (green), and 0.208 (pink). The dashed line indicates the response for  $A_p = 0$ . (b)  $n_s = 0.00926$  (pink), 0.023 (green), 0.0612 (light blue), and 0.129 (dark blue). The dashed line indicates the response for  $A_p = 0$ .

## V. VARIED SKYRMION DENSITIES

We next consider the effect of varying the skyrmion density for perpendicular driving. We expect that a series of commensurate and incommensurate transitions should occur as a function of the ratio of the skyrmion lattice spacing to the substrate lattice constant, as observed for superconducting vortex and colloidal systems; however, a study of such effects is outside the scope of the present work. In Fig. 16(a) we plot  $\langle V_{\perp} \rangle$  versus  $F_{\perp}^D$  for a system with  $\alpha_m/\alpha_d = 4.925$  and  $A_p = 0.5$  at  $n_s = 0.44, 0.36, 0.262$ , and 0.208. The dashed line is the result for  $A_p = 0$ , which is independent of  $n_s$ . The  $n_s = 0.208$  results are very similar to the behavior at  $n_s = 0.16$  shown in Fig. 8, where there is a drop in  $\langle V_{\perp} \rangle$  at the MS-ML transition and a cusp at the ML-MC transition. As  $n_s$  increases, the extent of the MS phase decreases and the onset of the MC phase shifts to higher values of  $F_{\perp}^D$ . For the higher values of  $n_s$ , the MS phase contains multiple rows of moving skyrmions per substrate minimum, as illustrated in Fig. 17(a) at  $n_s = 0.37$  and  $F_{\perp}^D = 0$ . Fig. 17(c) shows the particle trajectories in the moving locked phase at  $F_{\perp}^D = 0.02$  where the motion occurs in one-dimensional channels. The  $\langle V_{\perp} \rangle$  curves in Fig. 16 also show that the speed up effect observed in the single skyrmion limit remains robust when the skyrmion density increases. Just above the MS-ML phase transition for the  $n_s = 0.44, 0.37$ , and 0.262 curves in Fig. 16, there is a region in which a coexistence of MS and ML flow occurs, as illustrated in Fig. 17(d) for  $n_s = 0.37$  and  $F_{\perp}^D = 0.08$ . At high

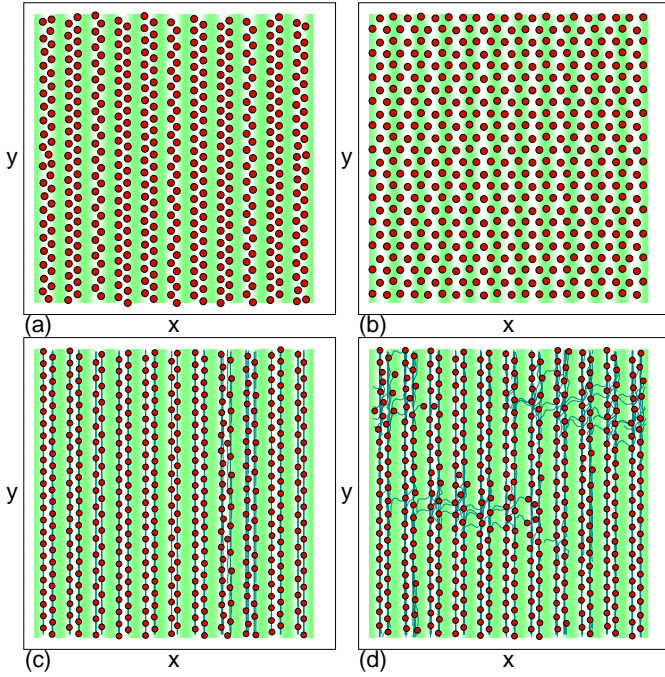


FIG. 17: Images of skyrmion locations (red dots) on the substrate potential (green) for the system in Fig. 16 with  $A_p = 0.5$  at  $n_s = 0.37$ . (a) Snapshot of the pinned state at  $F_{\perp}^D = 0$  where there are two rows of skyrmions per potential minima. (b) Snapshot of the moving crystal state at  $F_{\perp}^D = 0.5$ . (c) Skyrmion trajectories in the MS phase with two rows of moving skyrmions per potential minima at  $F_{\perp}^D = 0.02$ . (d) Skyrmion trajectories showing coexisting MS and ML flow at  $F_{\perp}^D = 0.08$ .

drives the system can dynamically order into the moving crystal phase, as shown in Fig. 17(b) for  $n_s = 0.37$  and  $F_{\perp}^D = 0.5$ . In Fig. 16(b) we plot  $\langle V_{\perp} \rangle$  versus  $F_{\perp}^D$  for the same system at  $n_s = 0.00926, 0.023, 0.0612,$  and  $0.129$ , where the dashed line shows the curve for a sample with  $A_p = 0$ . As  $n_s$  decreases, the extent of the ML phase is reduced while the ML-MS transition point remains almost constant. For  $n_s = 0.00926$ , the  $\langle V_{\perp} \rangle$  curve is almost the same as that found for the single skyrmion case, and there is no clear ML-MC transition.

In Fig. 18 we map the dynamic phase diagram as a function of  $F_{\perp}^D$  and  $n_s$ . The MS-ML transition line drops markedly above  $n_s = 0.25$  due to the formation of double rows of skyrmions in each substrate minimum in the MS phase, as illustrated in Fig. 17(a). Additionally, for  $n_s < 0.02$  the system behavior becomes identical to the single skyrmion limit. These results show that the skyrmion phases we observe should be robust over a wide range of magnetic fields.

We have also examined hysteretic effects across the different dynamic phase transitions by ramping the applied drive up and down, as shown in Fig. 19 where we plot  $\langle V_{\perp} \rangle$  and  $\langle V_{\parallel} \rangle$  versus  $F_{\perp}^D$  at  $A_p = 1.0$ ,  $n_s = 0.16$ , and  $\alpha_m/\alpha_d = 3.042$ . The thin line is the ramp up curve and the thick line is the ramp down curve. Hysteresis ap-

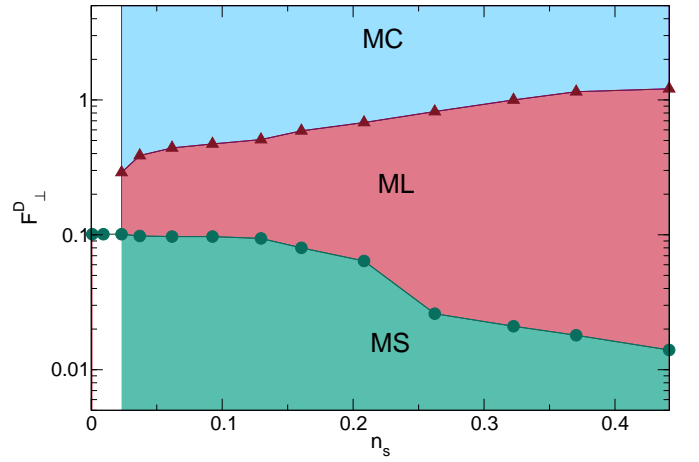


FIG. 18: The dynamic phase diagram for the system in Fig. 16 as a function of  $F_{\perp}^D$  and  $n_s$ . The MS-ML transition drops to lower values of  $F_{\perp}^D$  with increasing  $n_s$  once double rows of skyrmions can form in the potential minima, as illustrated in Fig. 17(a). For  $n_s < 0.02$ , the system behavior is the same as in the single skyrmion limit.

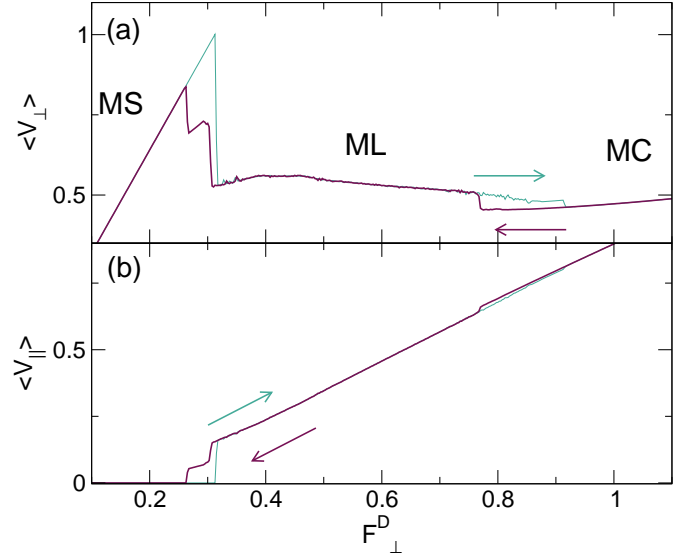


FIG. 19: (a)  $\langle V_{\perp} \rangle$  vs  $F_{\perp}^D$  for a system with  $n_s = 0.16$ ,  $A_p = 1.0$ , and  $\alpha_m/\alpha_d = 3.042$ . The thin green line indicates the ramp up and the thick red line indicates the ramp down, showing hysteresis across the MH-ML and ML-MS transitions. (b) The same for  $\langle V_{\parallel} \rangle$  vs  $F_{\perp}^D$ .

pears in both  $\langle V_{\parallel} \rangle$  and  $\langle V_{\perp} \rangle$  across the ML-MC phase transition, where the system remains locked in the moving crystal phase down to lower drives than that at which the MC phase first appears on the increasing portion of the ramp. There is also hysteresis across the ML-MS phase transition, where the system remains in the ML phase down to lower drives for the ramp down than during the ramp up. In general, we observe hysteresis for all values of  $\alpha_m/\alpha_d$ , with a slight increase in the width

of the hysteretic intervals for increasing  $\alpha_m/\alpha_d$ . This shows that several of the dynamic phases have first order like features, and that hysteresis in the transport curves provides another method for identifying the onset of the different dynamic phases.

## VI. SUMMARY

We have examined individual and multiple skyrmions in a 2D system driven over a quasi-1D periodic substrate where the Magnus term in the dynamics produces new effects that are not observed in overdamped realizations of this geometry. When the driving force is applied parallel to the substrate periodicity direction, the depinning force is not reduced when the magnitude of the Magnus force increases, in contrast to what occurs for pointlike pinning. This is because the planar nature of the quasi-1D pinning substrate does not allow the skyrmions to curve around and avoid the pinning sites, as is possible for pointlike pinning. For driving in the direction perpendicular to the substrate periodicity, in the overdamped limit the substrate potential has no effect and the velocity force curves are linear as the particles simply slide along the substrate. When a finite Magnus term is present, however, a rich variety of dynamical effects can arise. At lower external drives the skyrmion motion is locked to the direction of drive, while at higher drives there is a transition to motion both transverse and parallel to the applied drive. At this transition there is a decrease in the net skyrmion velocity, producing a negative differential conductivity effect. Within the longitudinally locked phase, there is a pronounced speed up effect in which the skyrmions move faster than particles in the overdamped

limit would move. This occurs when the velocity component from the Magnus term is aligned with the external drive. Such speed up effects were previously observed for systems with pointlike or circular pinning sites. Here we find a speed up effect only for perpendicular driving. For collectively interacting skyrmions, a variety of distinct dynamical phases arise including moving smectic, liquid, hexatic, and crystal phases. The transitions into and out of many of these phases produce dips and cusps in the transport curves. We map the onset of these different phases as a function of the ratio of the Magnus term to the dissipative term, the external drive, the substrate strength, and the skyrmion density. For varied substrate strengths we find evidence for an Aubry like transition when the substrate is weak enough that the skyrmions form a floating triangular solid. For increasing skyrmion density, we find a transition from one to multiple rows of skyrmions in each substrate minima, which coincides with a decrease in the range of driving force values over which skyrmion motion remains locked in the direction of the perpendicular driving force. A potential of the type we consider could be realized using samples with periodic thickness modulations or magnetic line pinning, or even via optical means, and the existence of different skyrmion dynamical phases could be deduced from changes in the transport curves or by observing dynamical changes of the skyrmion configurations.

## Acknowledgments

This work was carried out under the auspices of the NNSA of the U.S. DoE at LANL under Contract No. DE-AC52-06NA25396.

- 
- <sup>1</sup> A. Chowdhury, B. J. Ackerson, and N. A. Clark, Laser-induced freezing, *Phys. Rev. Lett.* **55**, 833 (1985).
- <sup>2</sup> Q.-H. Wei, C. Bechinger, D. Rudhardt, and P. Leiderer, Experimental study of laser-induced melting in two-dimensional colloids, *Phys. Rev. Lett.* **81**, 2606 (1998).
- <sup>3</sup> E. Frey, D. Nelson, and L. Radzihovsky, Light-induced melting of colloidal crystals in two dimensions, *Phys. Rev. Lett.* **83**, 2977 (1999).
- <sup>4</sup> L. Zaidouny, T. Bohlein, R. Roth, and C. Bechinger, Light-induced phase transitions of colloidal monolayers with crystalline order, *Soft Matter* **9**, 9230 (2013).
- <sup>5</sup> J. Hu and R. M. Westervelt, Commensurate-incommensurate transitions in magnetic bubble arrays with periodic line pinning, *Phys. Rev. B* **55**, 771 (1997).
- <sup>6</sup> S. Herrera-Velarde and R. Castañeda-Priego, Diffusion in two-dimensional colloidal systems on periodic substrates *Phys. Rev. E* **79**, 041407 (2009).
- <sup>7</sup> P. Tierno, Depinning and collective dynamics of magnetically driven colloidal monolayers, *Phys. Rev. Lett.* **109**, 198304 (2012).
- <sup>8</sup> O. Daldini, P. Martinoli, J.L. Olsen, and G. Berner, Vortex-line pinning by thickness modulation of superconducting films, *Phys. Rev. Lett.* **32**, 218 (1974).
- <sup>9</sup> P. Martinoli, Static and dynamic interaction of superconducting vortices with a periodic pinning potential, *Phys. Rev. B* **17**, 1175 (1978).
- <sup>10</sup> D. Jaquel, E. M. González, J.I. Martin, J. V. Anguita, and J. L. Vicent, Anisotropic pinning enhancement in Nb films with arrays of submicrometric Ni lines, *Appl. Phys. Lett.* **81**, 2851 (2002).
- <sup>11</sup> G. Karapetrov, M. Milosevic, M. Iavarone, J. Fedor, A. Belkin, V. Novosad, and F. Peeters, Transverse instabilities of multiple vortex chains in magnetically coupled NbSe<sub>2</sub>/permalloy superconductor/ferromagnet bilayers, *Phys. Rev. B* **80**, 180506 (2009).
- <sup>12</sup> O.V. Dobrovolskiy, E. Begun, M. Huth, and V.A. Shklovskij, Electrical transport and pinning properties of Nb thin films patterned with focused ion beam-milled washboard nanostructures, *New J. Phys.* **14**, 113027 (2012).
- <sup>13</sup> I. Guillamón, R. Córdoba, J. Sesé, J.M. De Teresa, M.R. Ibarra, S. Vieira, and H. Suderow, Enhancement of long-range correlations in a 2D vortex lattice by an incommensurate 1D disorder potential, *Nature Phys.* **10**, 851 (2014).

- <sup>14</sup> Q. Le Thien, D. McDermott, C. J. Olson Reichhardt, and C. Reichhardt, Orientational ordering, buckling, and dynamic transitions for vortices interacting with a periodic quasi-one-dimensional substrate, *Phys. Rev. B* **93**, 014504 (2016).
- <sup>15</sup> A. Vanossi, N. Manini, M. Urbakh, S. Zapperi, and E. Tosatti, Modeling friction: From nanoscale to mesoscale, *Rev. Mod. Phys.* **85**, 529 (2013).
- <sup>16</sup> C. Reichhardt and C. J. Olson Reichhardt, Pinning and dynamics of colloids on one-dimensional periodic potentials, *Phys. Rev. E* **72**, 032401 (2005).
- <sup>17</sup> M.P.N. Juniper, A.V. Straube, R. Besseling, D.G.A.L. Aarts, and R.P.A. Dullens, Microscopic dynamics of synchronization in driven colloids, *Nature Commun.* **6**, 7187 (2015).
- <sup>18</sup> C. Reichhardt, C.J. Olson, and F. Nori, Dynamic phases of vortices in superconductors with periodic pinning, *Phys. Rev. Lett.* **78**, 2648 (1997).
- <sup>19</sup> A.M. Lacasta, J.M. Sancho, A.H. Romero, and K. Lindenberg, Sorting on periodic surfaces, *Phys. Rev. Lett.* **94**, 160601 (2005).
- <sup>20</sup> J. Gutierrez, A.V. Silhanek, J. Van de Vondel, W. Gillijns, and V. Moshchalkov, Transition from turbulent to nearly laminar vortex flow in superconductors with periodic pinning, *Phys. Rev. B* **80**, 140514 (2009).
- <sup>21</sup> T. Bohlein, J. Mikhael, and C. Bechinger, Observation of kinks and antikinks in colloidal monolayers driven across ordered surfaces, *Nature Mater.* **11**, 126 (2012).
- <sup>22</sup> A. Vanossi, N. Manini, and E. Tosatti, Static and dynamic friction in sliding colloidal monolayers, *Proc. Natl. Acad. Sci. (U.S.A.)* **109**, 16429 (2012).
- <sup>23</sup> D. McDermott, J. Amelang, C. J. Olson Reichhardt, and C. Reichhardt, Dynamic regimes for driven colloidal particles on a periodic substrate at commensurate and incommensurate fillings, *Phys. Rev. E* **88**, 062301 (2013).
- <sup>24</sup> S. Mühlbauer, B. Binz, F. Jonietz, C. Pfleiderer, A. Rosch, A. Neubauer, R. Georgii, and P. Böni, Skyrmion lattice in a chiral magnet, *Science* **323**, 915 (2009).
- <sup>25</sup> X.Z. Yu, Y. Onose, N. Kanazawa, J.H. Park, J.H. Han, Y. Matsui, N. Nagaosa, and Y. Tokura, Real-space observation of a two-dimensional skyrmion crystal, *Nature* **465**, 901 (2010).
- <sup>26</sup> S. Heinze, K. von Bergmann, M. Menzel, J. Brede, A. Kubetzka, R. Wiesendanger, G. Bihlmayer, and S. Blügel, Spontaneous atomic-scale magnetic skyrmion lattice in two dimensions. *Nature Phys.* **7**, 713 (2011).
- <sup>27</sup> N. Nagaosa and Y. Tokura, Topological properties and dynamics of magnetic skyrmions, *Nature Nanotechnol.* **8**, 899 (2013).
- <sup>28</sup> W. Jiang, P. Upadhyaya, W. Zhang, G. Yu, M.B. Jungfleisch, F.Y. Fradin, J.E. Pearson, Y. Tserkovnyak, K.L. Wang, O. Heinonen, S.G.E. te Velthuis, and A. Hoffmann, Blowing magnetic skyrmion bubbles, *Science* **349**, 283 (2015).
- <sup>29</sup> G. Chen, A. Mascaraque, A.T. N'Diaye, and A.K. Schmid, Room temperature skyrmion ground state stabilized through interlayer exchange coupling, *Appl. Phys. Lett.* **106**, 242404 (2015).
- <sup>30</sup> Y. Tokunaga, X.Z. Yu, J.S. White, H.M. Rønnow, D. Morikawa, Y. Taguchi, and Y. Tokura, A new class of chiral materials hosting magnetic skyrmions beyond room temperature, *Nature Commun.* **6**, 7638 (2015).
- <sup>31</sup> O. Boulle, J. Vogel, H. Yang, S. Pizzini, D. de Souza Chaves, A. Locatelli, T.O. Mendes, A. Sala, L.D. Buda-Prejbeanu, O. Klein, M. Belmeguenai, Y. Roussigné, A. Stashkevich, S.M. Chérif, L. Aballe, M. Foerster, M. Chshiev, S. Auffret, I.M. Miron, and G. Gaudin, Room-temperature chiral magnetic skyrmions in ultrathin magnetic nanostructures, *Nature Nanotechnol.* **11**, 449 (2016).
- <sup>32</sup> S. Woo, K. Litzius, B. Krüger, M.-Y. Im, L. Caretta, K. Richter, M. Mann, A. Krone, R.M. Reeve, M. Weigand, P. Agrawal, I. Lemesch, M.-A. Mawass, P. Fischer, M. Kläui, and G.S.D. Beach, Observation of room temperature magnetic skyrmions and their current-driven dynamics in ultrathin metallic ferromagnets, *Nature Mater.* **15**, 501 (2016).
- <sup>33</sup> A. Fert, V. Cros, and J. Sampaio, Skyrmions on the track, *Nature Nanotechnol.* **8**, 152 (2013).
- <sup>34</sup> F. Jonietz, S. Mühlbauer, C. Pfleiderer, A. Neubauer, W. Münzer, A. Bauer, T. Adams, R. Georgii, P. Böni, R.A. Duine, K. Everschor, M. Garst, and A. Rosch, Spin transfer torques in MnSi at ultralow current densities, *Science* **330**, 1648 (2010).
- <sup>35</sup> J. Zang, M. Mostovoy, J.H. Han, and N. Nagaosa, Dynamics of skyrmion crystals in metallic thin films, *Phys. Rev. Lett.* **107**, 136804 (2011).
- <sup>36</sup> T. Schulz, R. Ritz, A. Bauer, M. Halder, M. Wagner, C. Franz, C. Pfleiderer, K. Everschor, M. Garst, and A. Rosch, Emergent electrodynamics of skyrmions in a chiral magnet, *Nature Phys.* **8**, 301 (2012).
- <sup>37</sup> D. Liang, J.P. DeGrave, M.J. Stolt, Y. Tokura, and S. Jin, Current-driven dynamics of skyrmions stabilized in MnSi nanowires revealed by topological Hall effect, *Nature Commun.* **6**, 8217 (2015).
- <sup>38</sup> X.Z. Yu, N. Kanazawa, W.Z. Zhang, T. Nagai, T. Hara, K. Kimoto, Y. Matsui, Y. Onose, and Y. Tokura, Skyrmion flow near room temperature in an ultralow current density, *Nature Commun.* **3**, 988 (2012).
- <sup>39</sup> J. Iwasaki, M. Mochizuki, and N. Nagaosa, Universal current-velocity relation of skyrmion motion in chiral magnets, *Nature Commun.* **4**, 1463 (2013).
- <sup>40</sup> S.-Z. Lin, C. Reichhardt, C.D. Batista, and A. Saxena, Particle model for skyrmions in metallic chiral magnets: Dynamics, pinning, and creep, *Phys. Rev. B* **87**, 214419 (2013).
- <sup>41</sup> C. Reichhardt, D. Ray, and C. J. Olson Reichhardt, Quantized transport for a skyrmion moving on a two-dimensional periodic substrate, *Phys. Rev. B* **91**, 104426 (2015).
- <sup>42</sup> J. Müller and A. Rosch, Capturing of a magnetic skyrmion with a hole, *Phys. Rev. B* **91**, 054410 (2015).
- <sup>43</sup> C. Reichhardt, D. Ray, and C.J. Olson Reichhardt, Collective transport properties of driven skyrmions with random disorder, *Phys. Rev. Lett.* **114**, 217202 (2015).
- <sup>44</sup> W. Jiang, X. Zhang, G. Yu, W. Zhang, M.B. Jungfleisch, J.E. Pearson, O. Heinonen, K.L. Wang, Y. Zhou, A. Hoffmann, and S.G.E. te Velthuis, Direct observation of the skyrmion Hall effect, arXiv:1603.07393 (unpublished).
- <sup>45</sup> C. Reichhardt and C. J. Olson Reichhardt, Shapiro steps for skyrmion motion on a washboard potential with longitudinal and transverse ac drives, *Phys. Rev. B* **92**, 224432 (2015).
- <sup>46</sup> M.P. Shaw, V.V. Mitin, E. Schöll, and H.L. Grubin, *The Physics of Instabilities in Solid State Electron Devices* (Plenum, London, 1992).
- <sup>47</sup> H. Asai and S. Watanabe, Vortex dynamics and critical current in superconductors with unidirectional twin boundaries, *Phys. Rev. B* **77**, 224514 (2008).
- <sup>48</sup> C. Reichhardt and C.J. Olson Reichhardt, Pinning and dy-

- namics of colloids on one-dimensional periodic potentials, *Phys. Rev. E* **72**, 032401 (2005).
- <sup>49</sup> O.M. Braun, T. Dauxois, M.V. Paliy, and M. Peyrard, Dynamical transitions in correlated driven diffusion in a periodic potential, *Phys. Rev. Lett.* **78**, 1295 (1997).
- <sup>50</sup> C. Reichhardt and C. J. Olson Reichhardt, Spontaneous transverse response and amplified switching in superconductors with honeycomb pinning arrays, *Phys. Rev. Lett.* **100**, 167002 (2008).
- <sup>51</sup> C. Reichhardt and C.J. Olson Reichhardt, Moving vortex phases, dynamical symmetry breaking, and jamming for vortices in honeycomb pinning arrays, *Phys. Rev. B* **78**, 224511 (2008).
- <sup>52</sup> S. Bhattacharya and M.J. Higgins, Dynamics of a disordered flux line lattice, *Phys. Rev. Lett.* **70**, 2617 (1993).
- <sup>53</sup> A.E. Koshelev and V.M. Vinokur, Dynamic melting of the vortex lattice, *Phys. Rev. Lett.* **73**, 3580 (1994).
- <sup>54</sup> C.J. Olson, C. Reichhardt, and F. Nori, Nonequilibrium dynamic phase diagram for vortex lattices, *Phys. Rev. Lett.* **81**, 3757 (1998).
- <sup>55</sup> A. Kolton, D. Domínguez, and N. Grønbech-Jensen, Hall noise and transverse freezing in driven vortex lattices, *Phys. Rev. Lett.* **83**, 3061 (1999).
- <sup>56</sup> S. Aubry and P.Y. Le Daeron, The discrete Frenkel-Kontorova model and its extensions: I. Exact results for the ground-states, *Physica D* **8**, 381 (1983).
- <sup>57</sup> D. Mandelli, A. Vanossi, M. Invernizzi, S.V.P. Ticco, N. Manini, and E. Tosatti, Superlubric-pinned transition in sliding incommensurate colloidal monolayers, arXiv:1508.00147 (unpublished).